The Consequences of the Phosphine Steric and Electronic Profile in the Rh-Catalysed dehydrocoupling of Phosphine-Boranes

Thomas N. Hooper,[a] Miguel A. Huertos,[a] Sebastian D. Pike,[a] Titel Jurca,[b] Andrew S. Weller*[a] and Ian Manners[b]

a) Department of Chemistry, Inorganic Chemistry Laboratories, South Parks Road, University of Oxford, Oxford, OX1 3QR, UK.

b) School of Chemistry, University of Bristol, Cantock's Close, Bristol, BS8 1TS, UK.

Selected NMR spectroscopy ESI-MS data **S-2**

14 → **17** + **21**. Characterization of intermediate **20** by NMR spectroscopy **S-10**

Kinetic Studies **S-13**

Crystallography **S-16**

References **S-19**

Selected NMR spectroscopy and ESI-MS data

14

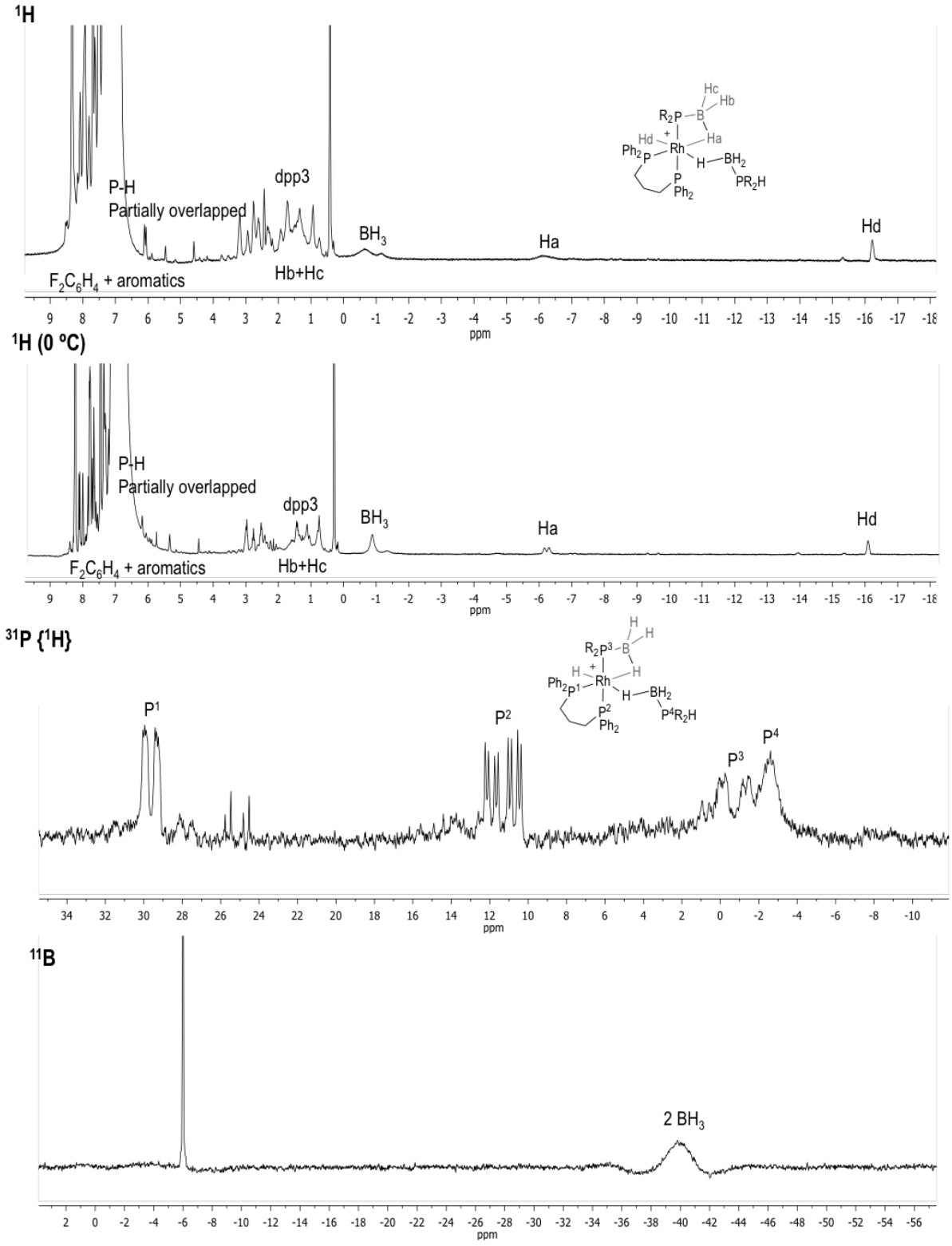

Figure S1: ^{1}H, $^{31}P\{^{1}H\}$ and ^{11}B NMR spectra for compound **14.**

17

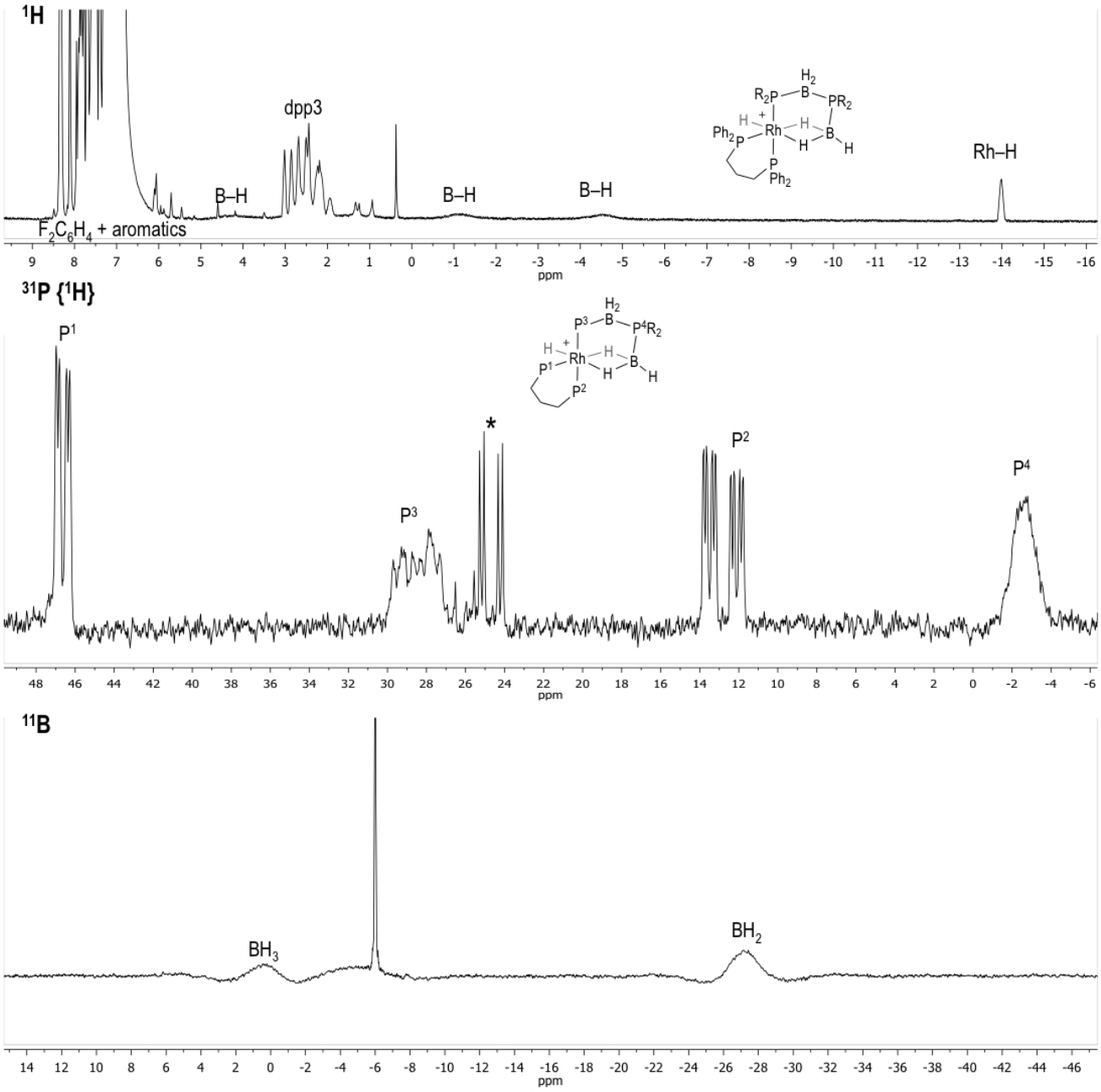

Figure S2: ^{1}H, $^{31}P\{^{1}H\}$ and ^{11}B NMR spectra for compound **17.**

24

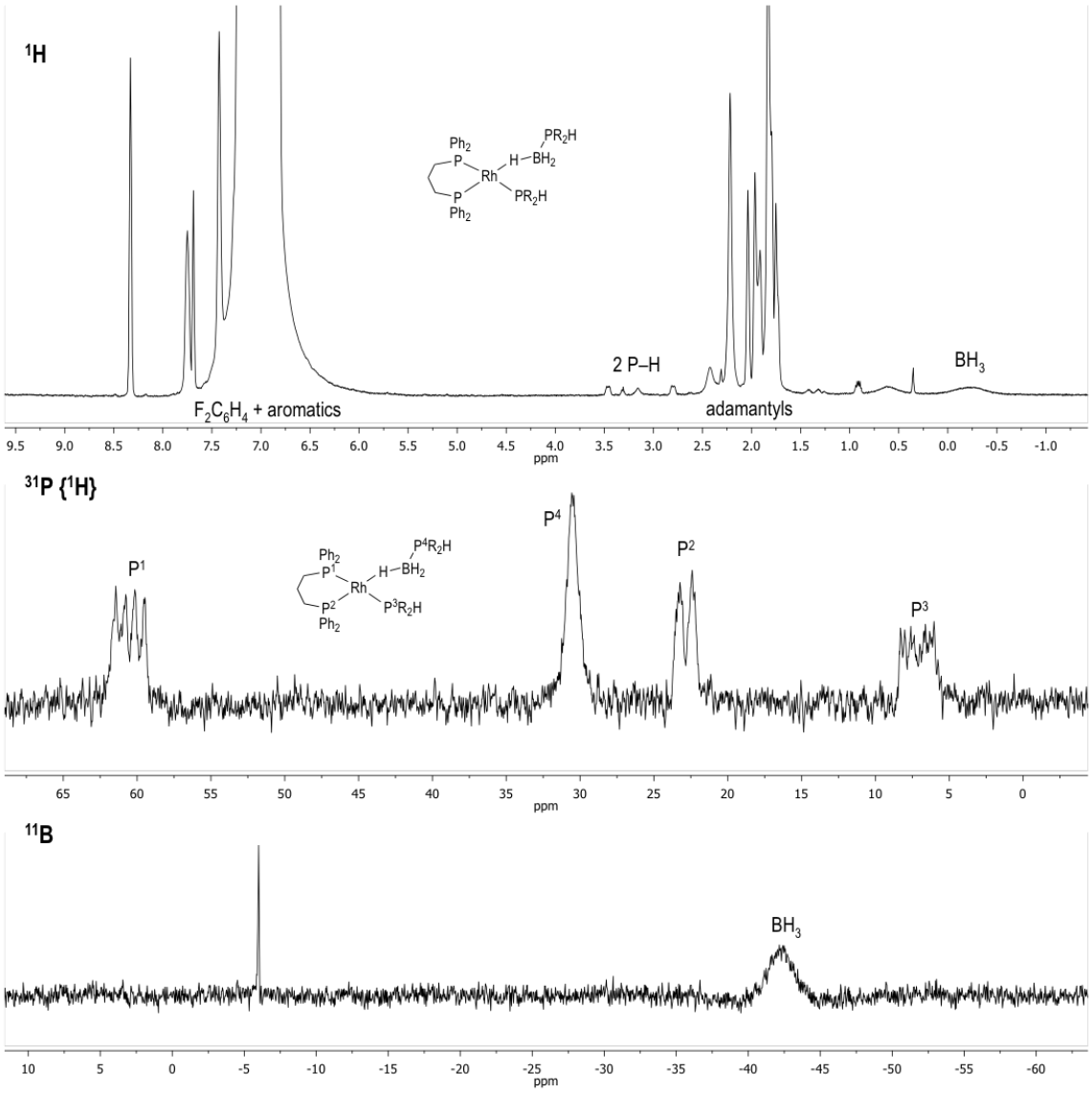

Figure S3: ^{1}H, $^{31}P\{^{1}H\}$ and ^{11}B NMR spectra for compound **24.**

25a and 25b

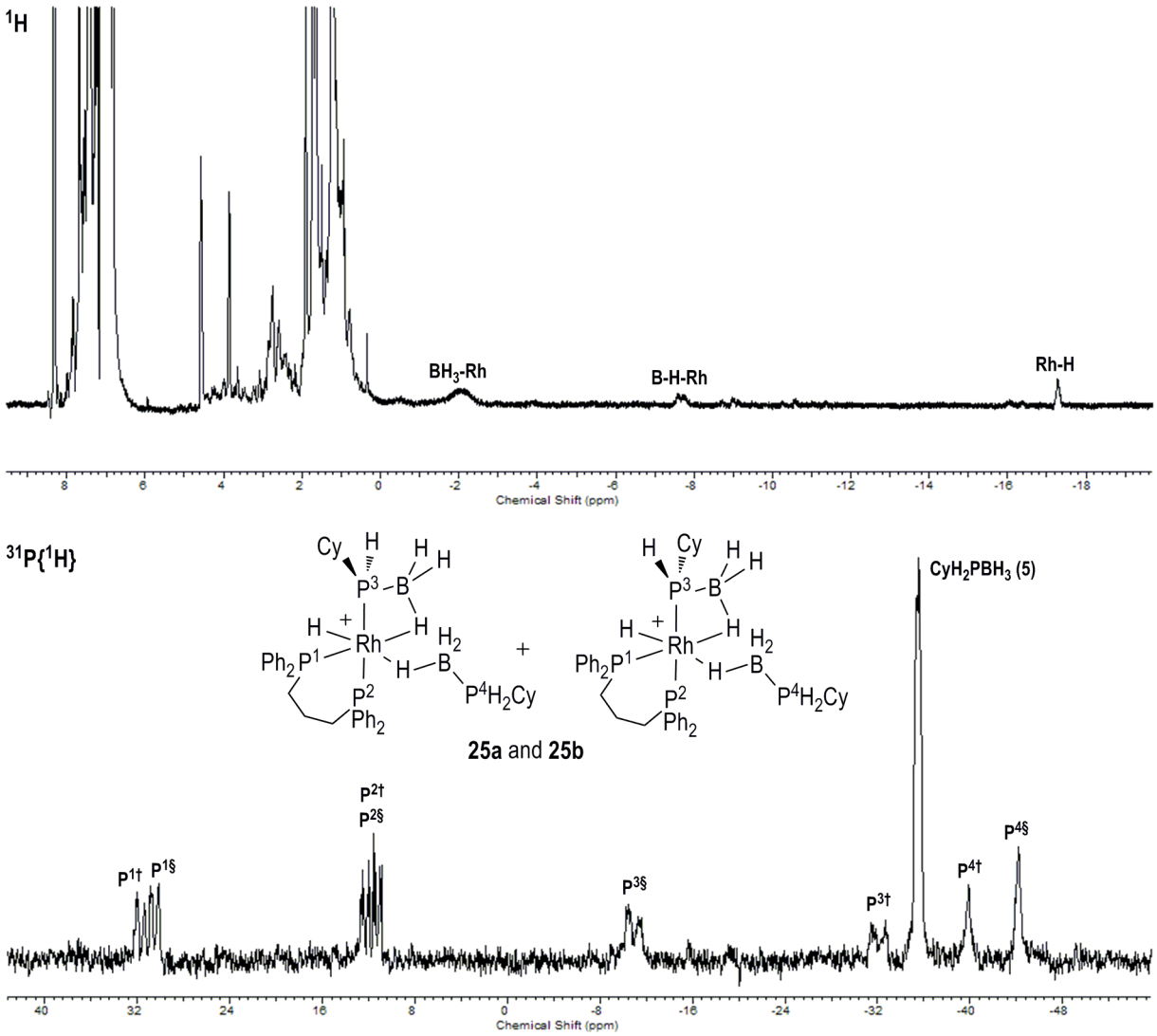

Figure S4: ^{1}H and $^{31}P\{^{1}H\}$ NMR spectra for compounds **25a** and **25b.** 2 diastereomers are present, while we were able to identify the 2 sets of 4 resonances (labelled † and §, based on coupling constants and approximate integrations) it was not possible to determine which set of signals belonged to which diastereomer.

26a and 26b

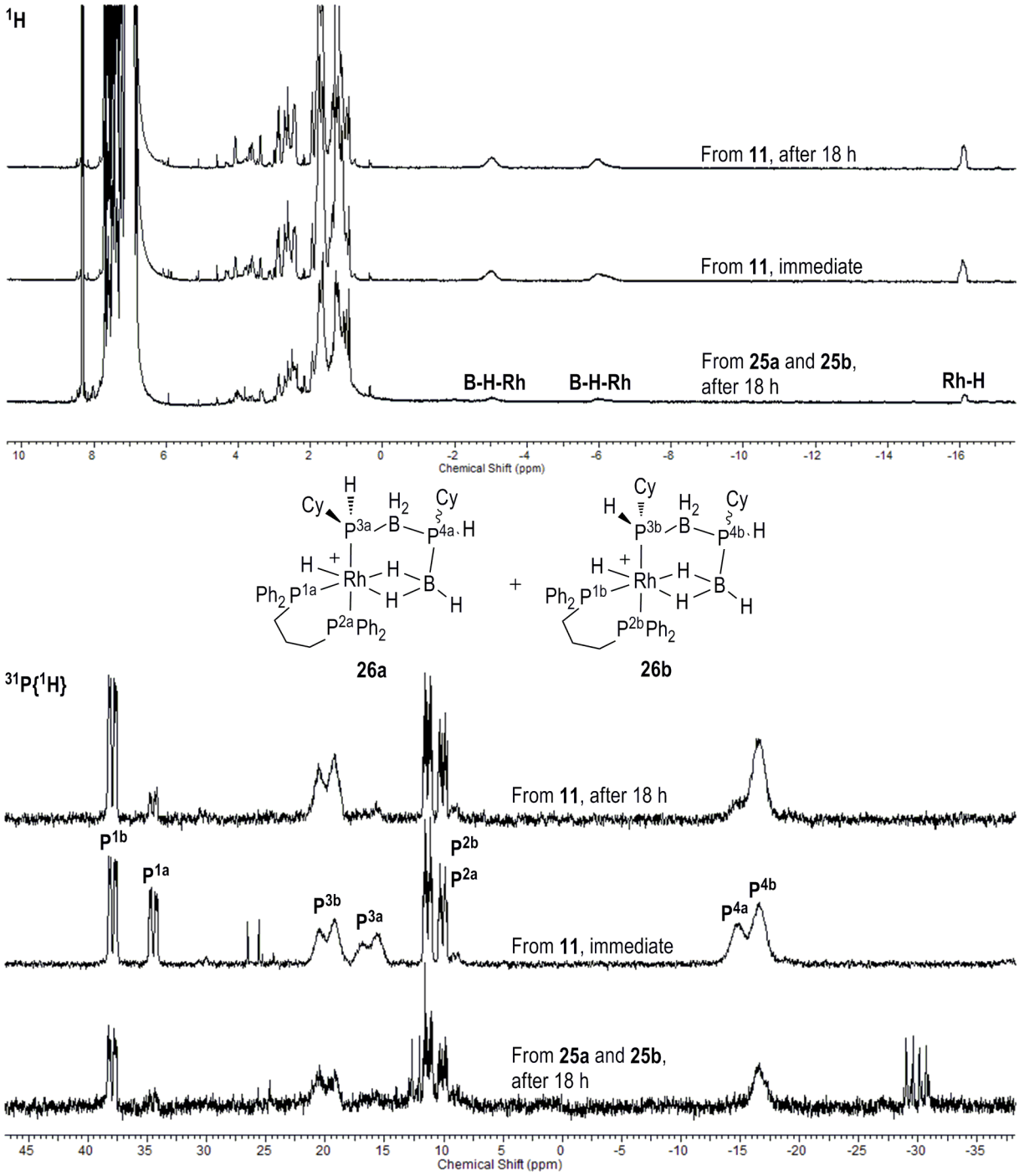

Figure S5: ^{1}H and $^{31}P\{^{1}H\}$ NMR spectra for compounds **26a** and **26b.** The $^{31}P\{^{1}H\}$ NMR spectrum of this reaction mixture indicates that 2 diastereomers are present, we were able to identify the 2 sets of 4 resonances (labelled **a** and **b**, based on coupling constants and approximate integrations) and assigned the diastereomers (scheme S5) by inspection of a model.

27a and 27b

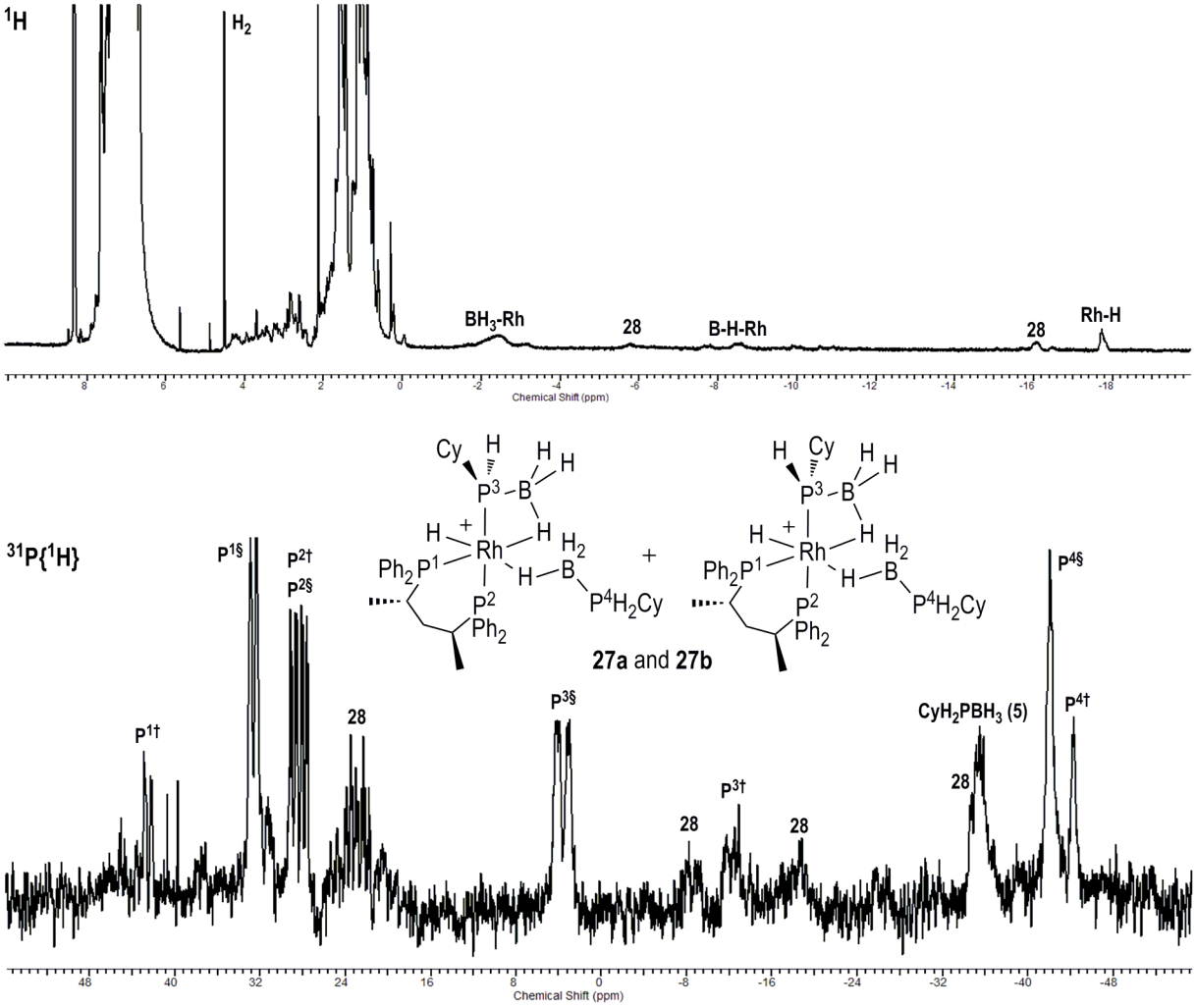

Figure S6: ^{1}H and $^{31}P\{^{1}H\}$ NMR spectra for compounds **27a** and **27b.** 2 diastereomers are present, while we were able to identify the 2 sets of 4 resonances (labelled † and §, based on coupling constants and approximate integrations) it was not possible to determine which set of signals belonged to which diastereomer. The dehydrocoupling reaction proceeded very rapidly and small traces of compounds of **28** can be observed in both the ^{1}H and $^{31}P\{^{1}H\}$ NMR spectra and have been labelled, as well a sharp singlet for dihydrogen in the ^{1}H NMR spectrum at δ 4.53.

28a, 28b, 28c and 28d

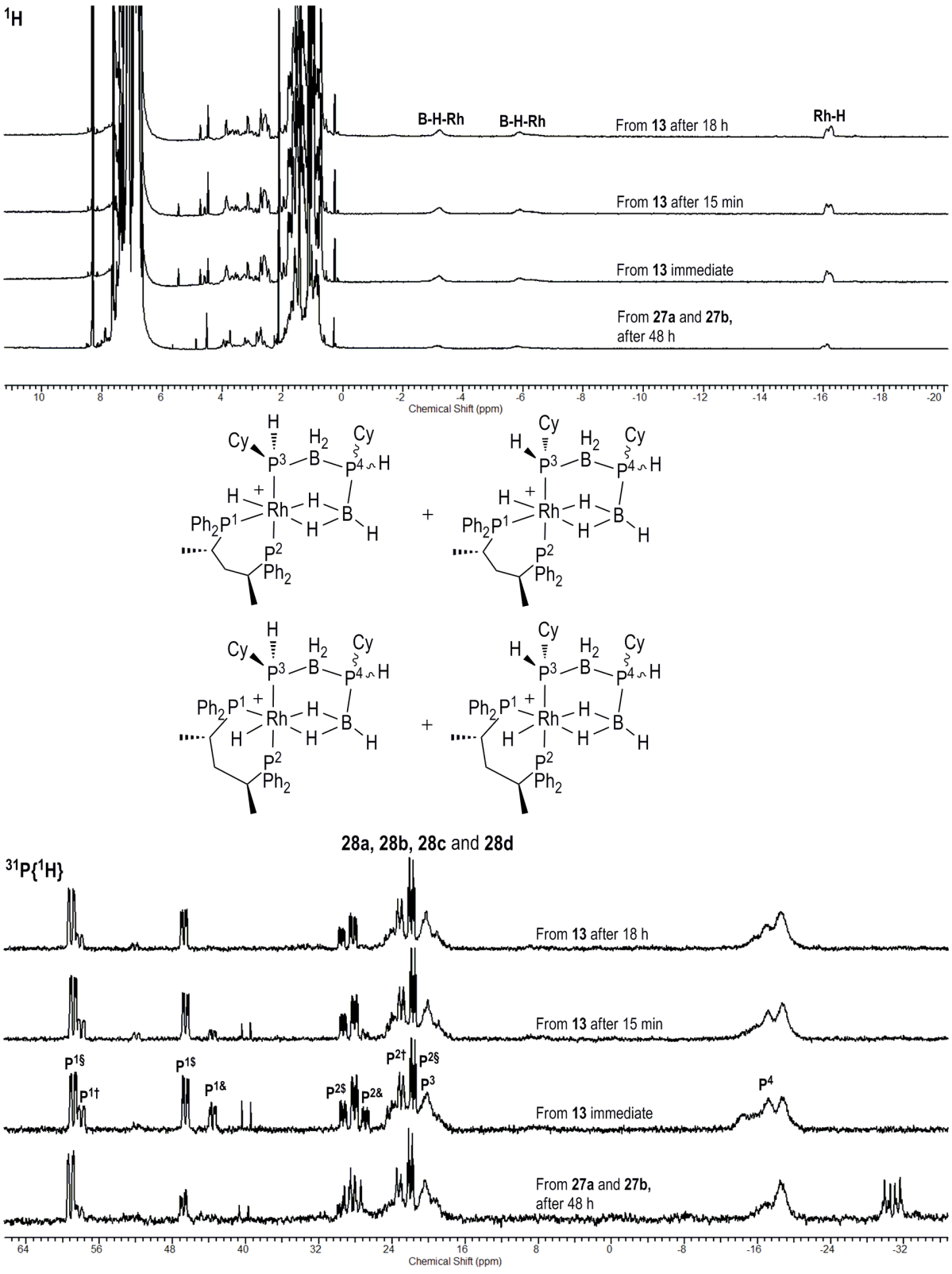

Figure S7: ^{1}H and $^{31}P\{^{1}H\}$ NMR spectra for compounds **28a**, **28b**, **28c** and **28d.** 4 diastereomers are present, while we were able to identify the 4 sets of 4 resonances (labelled †, §, $ and & based on coupling constants and approximate integrations) some of which overlap it was not possible to determine which set of signals belonged to which diastereomer.

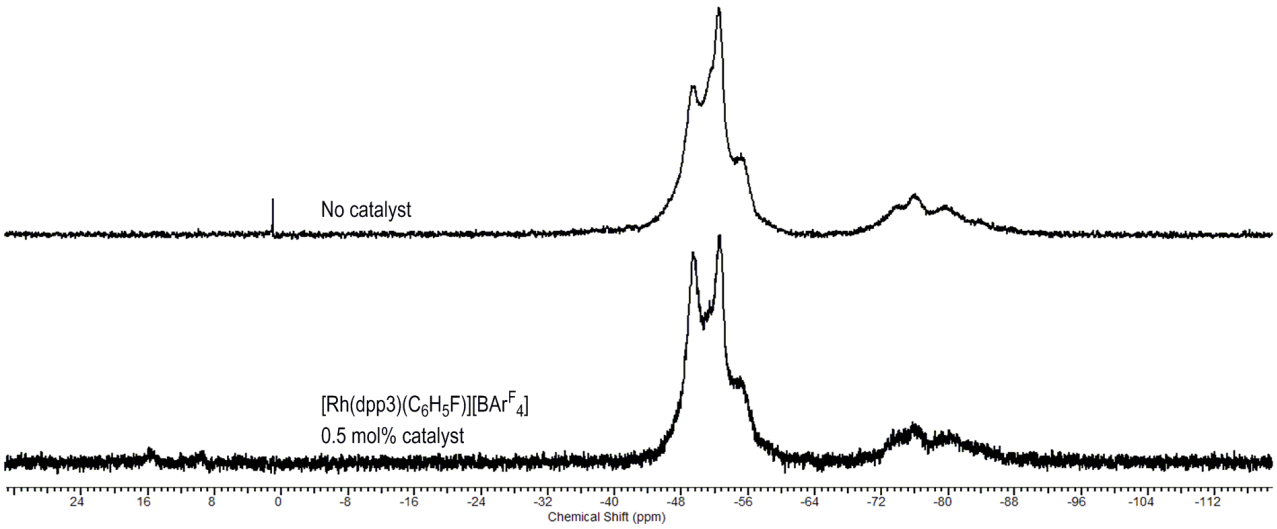

Figure S8: $^{31}P\{^{1}H\}$ NMR spectra of isolated products of attempted solution phase polymerisation of $PhH_2P{\cdot}BH_3$ in toluene heated to reflux using $[Rh(dpp3)(C_6H_5F)][BAr^F{}_4]$ as a catalyst (bottom) and no catalyst (top).

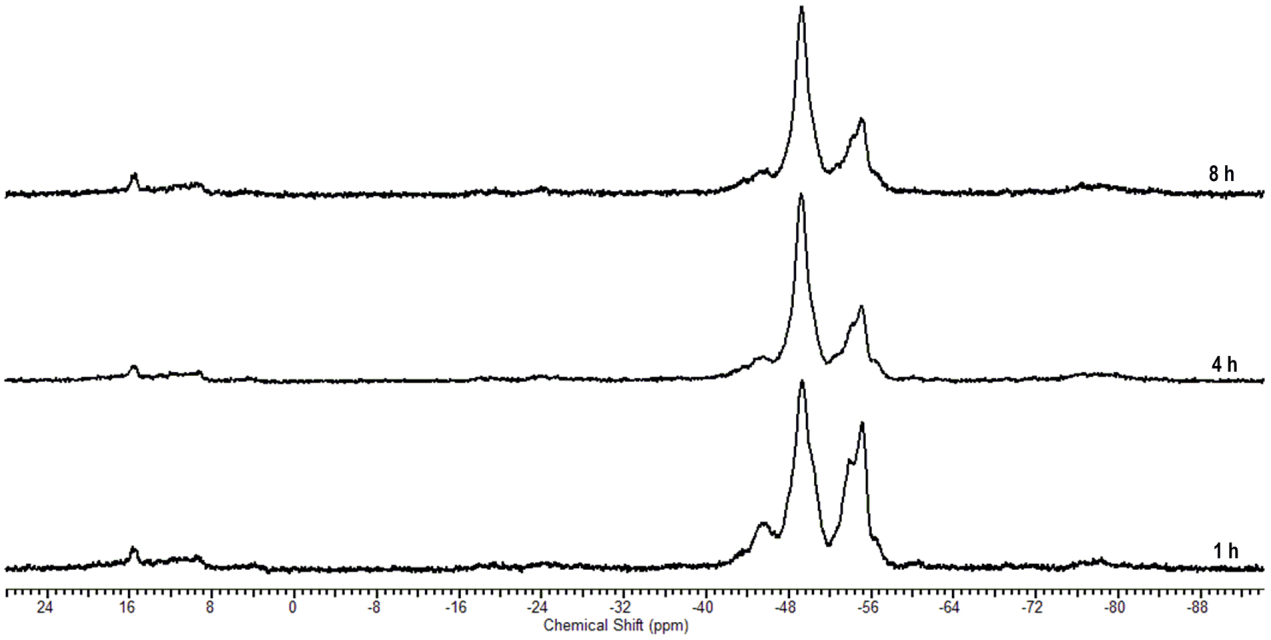

Figure S9: $^{31}P\{^{1}H\}$ NMR spectra of dissolved reaction mixtures of melt polymerisations of $PhH_2P{\cdot}BH_3$ in using 5 mol% $[Rh(dpp3)(C_6H_5F)][BAr^F{}_4]$ as a catalyst after 1, 4 and 8 hours.

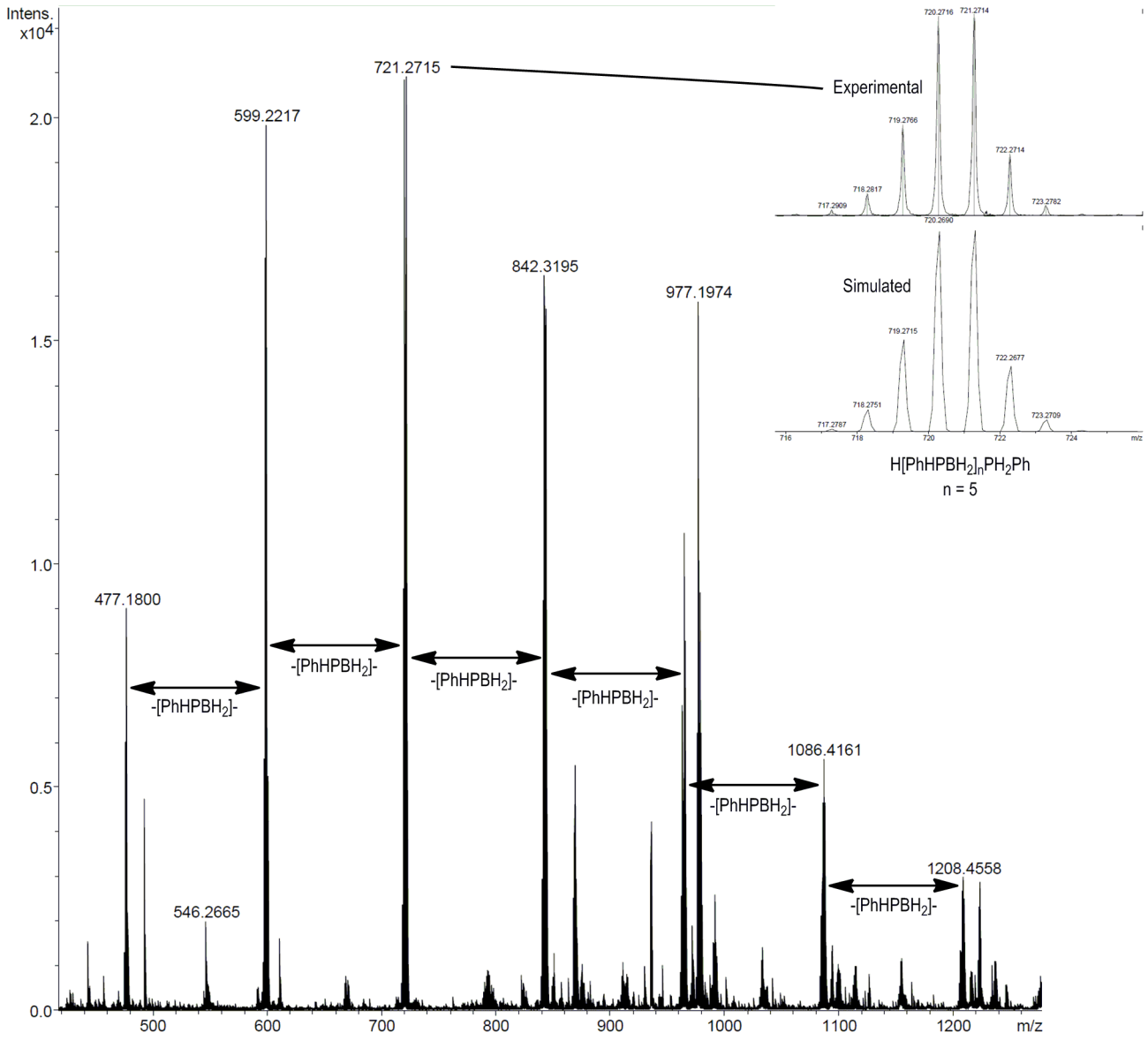

Figure S10: ESI mass spectrum of the reaction mixture of the melt polymerisation of $PhH_2P{\cdot}BH_3$ after 1 hour dissolved in 1,2-difluorobenzene showing a regular repeating pattern of -[$PhHP{\cdot}BH_2$]- units observed as *cationic* $[H[PhHP{\cdot}BH_2]_nPH_2Ph]^+$ up to n = 10.

14 ⟶ 17 + 21. Characterisation of intermediate 20 by NMR spectroscopy

Compound **14** reacts to form a mixture (1:1 approximate ratio) of **17** and **21**. Following this reaction by NMR spectroscopy we were able to characterise an intermediate, **20**, in the formation of **21**. Compound **14** can react in two ways; the first (way **A**, Scheme S1) is the dehydrocoupling and the formation of compound **17**. The second (way **B**, Scheme S1) is a two step process with two P–B bond cleavages. The first P–B bond cleavage leads to the formation of **20**, which has a short lifetime because it then rapidly undergoes another P–B bond cleavage to form **21**.

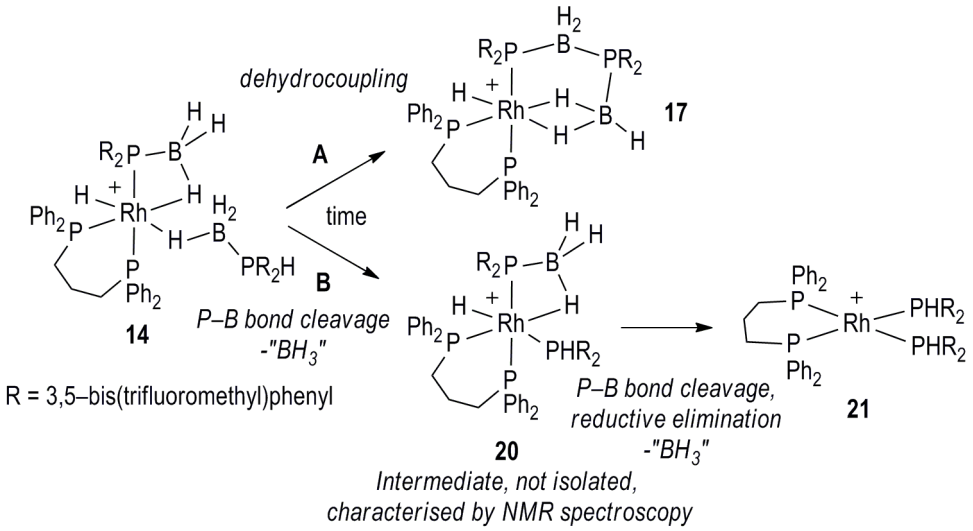

Scheme S1: Routes to the formation of compounds **17**, **20** and **21**.

Figure S11 shows the ^{1}H and $^{31}P\{^{1}H\}$ NMR spectra of compound **14** after 120 minutes stirring at room temperature. The ^{1}H NMR spectrum (top) shows a mixture between the starting product **14**, the dehydrocoupling product **17** and the intermediate **20**. The ^{1}H NMR spectrum for the intermediate **20** shows two doublets, one of them (δ -9.61, $J_{HP(trans)}$ = 165 Hz) corresponds to the hydride Rh–H^{d} and shows a coupling constant indicative for a hydride in the *trans*-position to a phosphine ligand. The other signal, a broad doublet (δ -7.06, $J_{HP(trans)}$ = 76 Hz) corresponds to H^{a} with a coupling constant indicative of the *trans* disposition of this hydrogen atom to one of the phosphorous atoms of the dpp3 ligand. The $^{31}P\{^{1}H\}$ NMR spectrum (bottom) of this mixture shows four different phosphorus environments for complex **20**. One of the resonances (δ -8.6, d, J_{PP} = 220 Hz, P^{3}) is a broad doublet suggesting one of the phosphorous atoms is bound to a quadrupolar ^{11}B centre and *trans* to another phosphorous of the dpp3 ligand (P^{2}). Another environment (δ 0.6, d, J_{PRh} = 90 Hz, P^{4}) is assigned to the bis[3,5-di(trifluoromethyl)phenyl] phosphine coordinated to the metal centre. The other two signals are assigned to the environments of the $Ph_2P(CH_2)_3PPh_2$ (dpp3) ligand (δ 27.5, d, J_{PRh} = 114 Hz, P^{1} and; δ 4.5, ddd, $J_{PP(trans)}$ = 220 Hz, J_{PRh} = 90 Hz, $J_{PP(cis)}$ = 30 Hz, P^{2}).

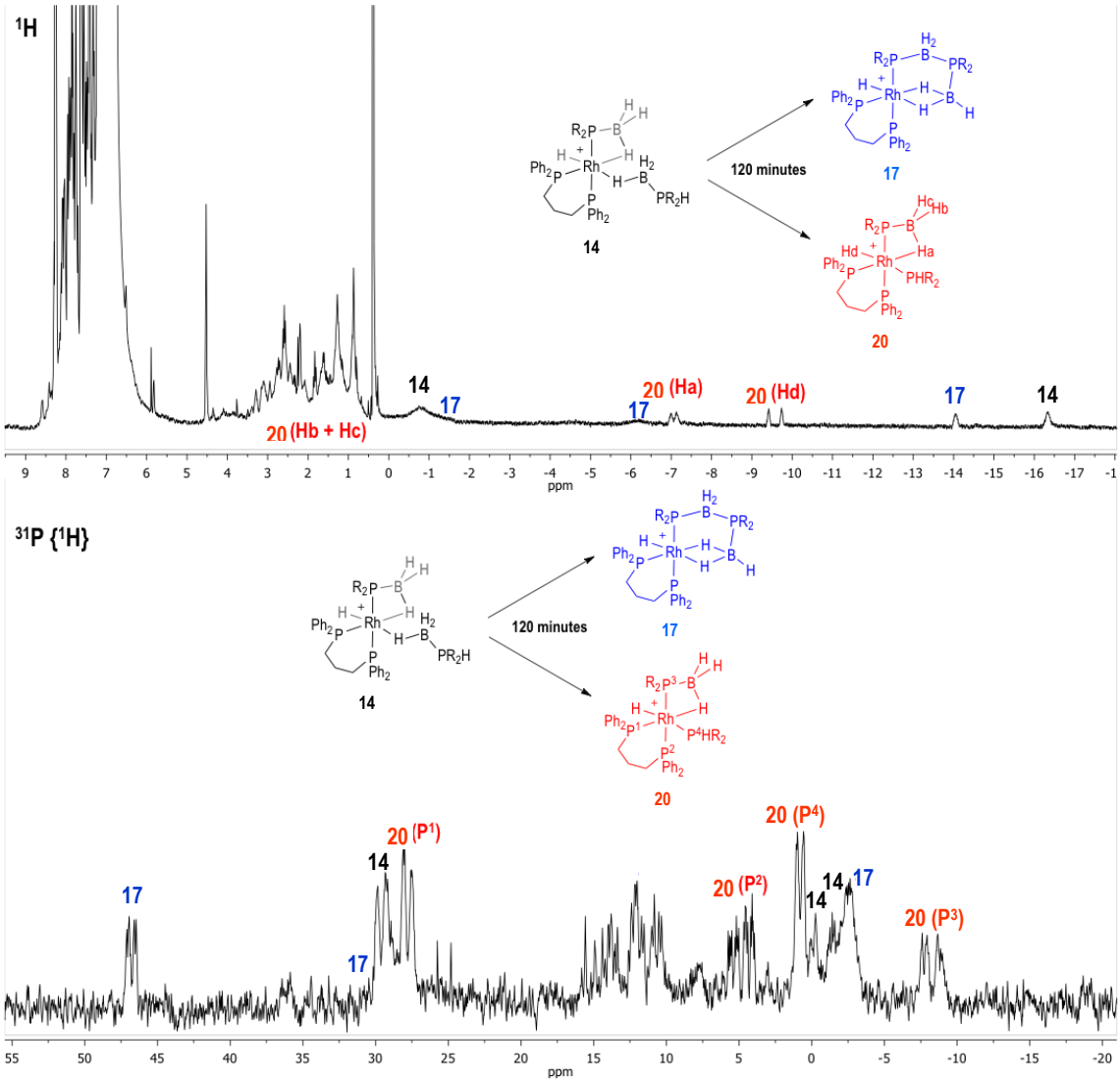

Figure S11: ^{1}H NMR spectrum in 1,2–$F_2C_6H_4$ of **14**, **17** and **20** (top); $^{31}P\{^{1}H\}$ NMR spectrum in 1,2–$F_2C_6H_4$ of **14**, **17** and **20** (bottom) after 120 minutes.

In a 2-dimensional correlation NMR experiment between the ^{1}H and ^{31}P nuclei, we observed that P^3HR_2 is BH_3 free (after P-B bond cleavage) because the signal for the P-**H^{e}** (which is correlated with P^3) is a sharp signal which indicates that P^3 is no longer bonded to a quadrupolar ^{11}B nucleus (Figure S12).

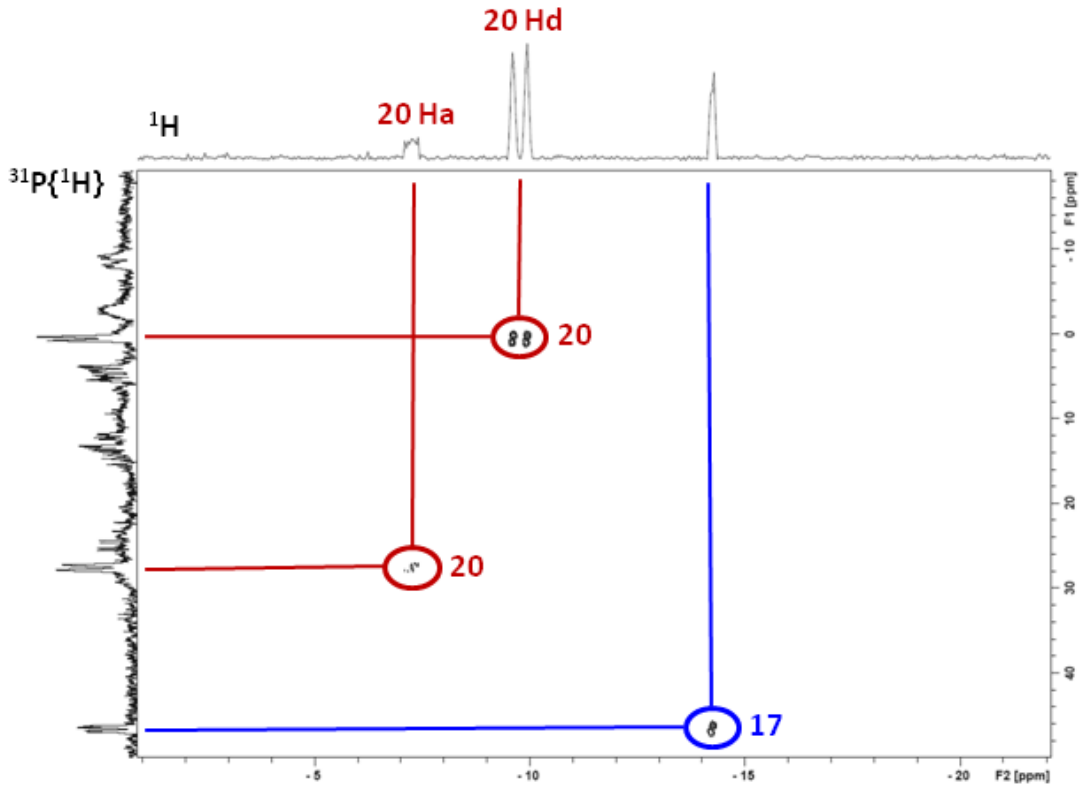

Figure S12: ^{1}H-^{31}P{^{1}H} correlation NMR spectrum in 1,2–$F_2C_6H_4$ of **14**, **17** and **20**.

Kinetic Studies

14 → 17 + 21 (298 K)

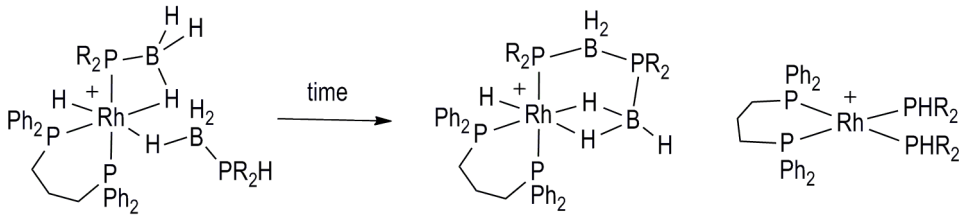

14 **17** **21**

R = 3,5-bis(trifluoromethyl)phenyl

Scheme S2: Formation of compounds **17** and **21** from **14**. $[BAr^{F}_4]^-$ anions not shown.

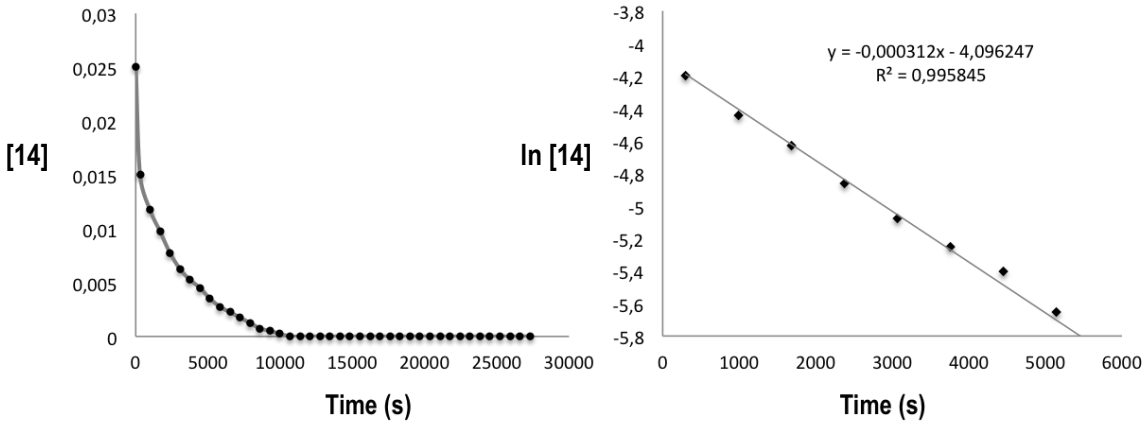

Figure S13: Concentration *vs* time and ln(concentration) *vs* time plots showing the disappearance of **14**.

15 → 18 + 22 (298 K)

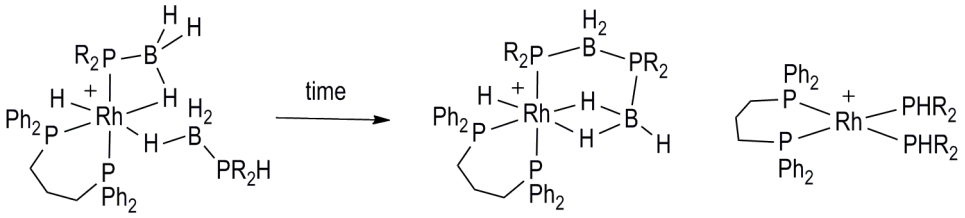

15
R = 4-(trifluoromethyl)phenyl

18

22

Scheme S3: Formation of compounds **18** and **22** from **15**. $[BAr^F_4]^-$ anions not shown.

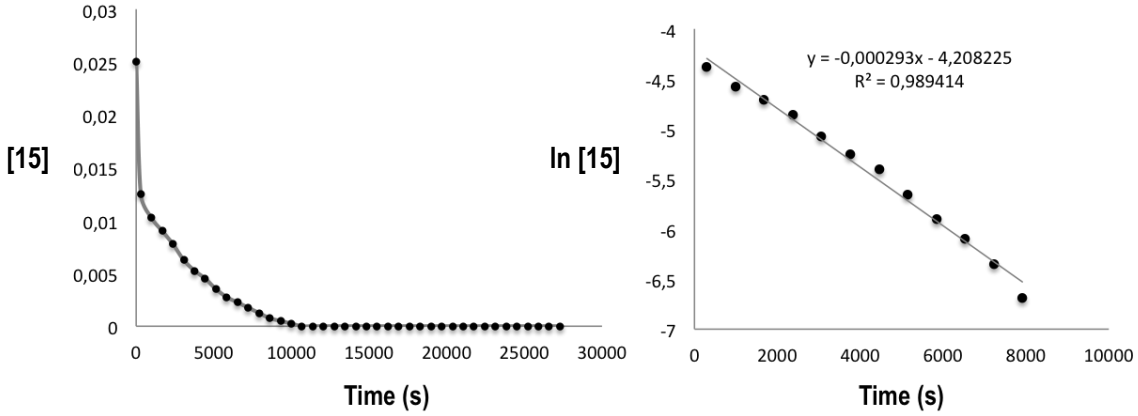

Figure S14: Concentration *vs* time and ln(concentration) *vs* time plots showing the disappearance of **15**.

16 → 19 (308 K)

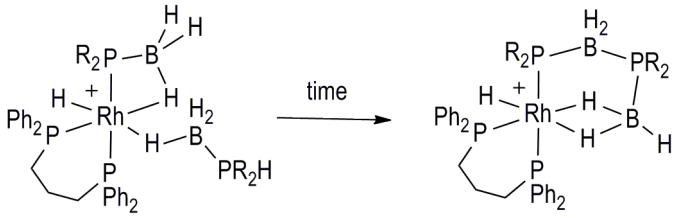

16 **19**

R = 4-methoxyphenyl

Scheme S4: Formation of compound **19** from **16**. $[BAr^F{}_4]^-$ anions not shown.

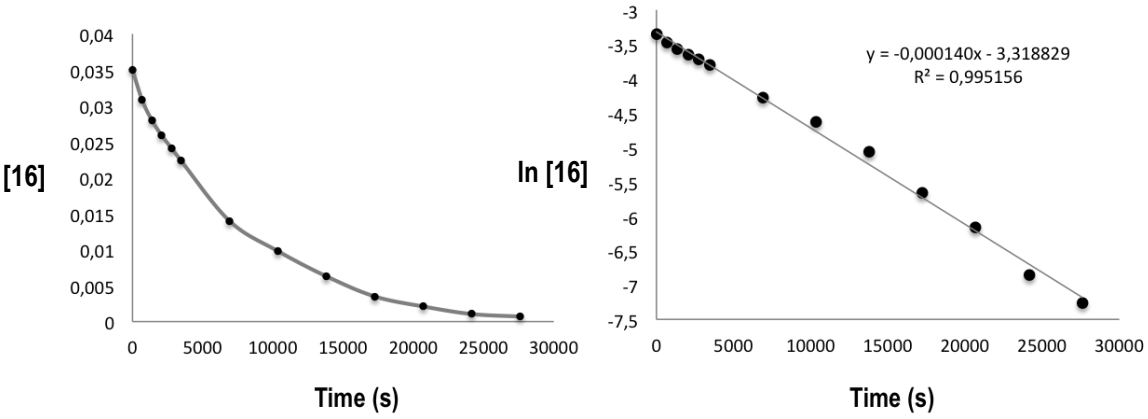

Figure S15: Concentration *vs* time and ln(concentration) *vs* time plots showing the disappearance of **16**.

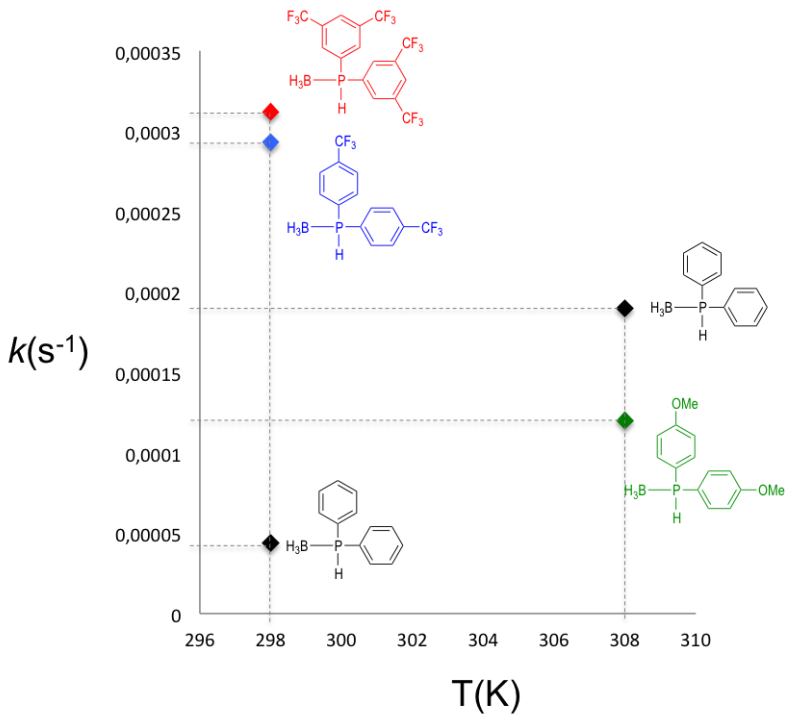

.

Figure S16: Plot showing relative rates of disappearance of [Rh(dpp3)H(PR_2·BH_3)(H_3B·PHR_2)][BAr^F_4] through dehydrocoupling and decomposition pathways at different temperatures.

Crystallography

X-ray crystallography data for compounds **14** and **13** was collected on an Enraf Nonius Kappa CCD diffractometer using graphite monochromated Mo Kα radiation (λ = 0.71073 Å) and a low-temperature device [150(2) K];[1] data were collected using COLLECT, reduction and cell refinement was performed using DENZO/SCALEPACK.[2] The structure of **14** was solved by charge flipping methods using Superflip[3] and refined full-matrix least squares on F^2 using CRYSTALS.[4] X-ray crystallography data for **17** and **24** was collected on an Agilent SuperNova diffractometer using graphite monochromated Cu Kα radiation (λ = 1.54180 Å) and a low-temperature device [150(2) K]; data were collected using SuperNova, reduction and cell refinement was performed using CrysAlis.[5] The structure was solved by charge flipping methods using Superflip and refined full-matrix least squares on F^2 using CRYSTALS. The structure of **13** was solved by direct methods (SHELXS-97) and refined by full matrix least squares using SHELXL-97.[6] All non-hydrogen atoms were refined with anisotropic displacement parameters. All hydrogen atoms were placed in calculated positions using the riding model unless stated otherwise. Crystallographic data have been deposited with the Cambridge Crystallographic Data Centre under **CCDC** 970085-8. These data can be obtained free of charge from the Cambridge Crystallographic Data Centre via www.ccdc.cam.ac.uk/data_request/cif.

Special details

Compound 14

Three solvent molecules of difluorobenzene were located during the refinement. They were restrained to each other in order to maintain sensible geometries. The occupancy of one difluorobenzene which displayed large thermal ellipsoids was refined to 0.614. The resulting model shows slightly larger thermal ellipsoids for the solvent molecules indicating minor disorder is present.

Rotational disorder of several CF_3 groups upon the phosphine substituents and the anion were treated by modelling the fluorine atoms over two sites and restraining their geometry.

H(1)-H(7) were located upon the fourier map and allowed to refine freely at first before ride restraints were applied.

Compound 17

Solvent molecules of difluorobenzene and pentane were located in the refinement. The pentane molecule was modelled and restrained to maintain sensible geometries. The disordered difluorobenzene solvent molecule could not be adequately modelled and and so was treated using the SQUEEZE algorithm.[7]

Rotational disorder of several CF_3 groups upon the "P-B-P-B" ligand and the anion was treated by modelling the fluorine atoms over two sites and restraining their geometry. H1, H4, H5, H6 were located upon the fourier map and allowed to refine freely before ride restraints were applied.

Compound 24

Orange crystals became cracked when removed from solvent presumably through solvent release, this lead to a high mosaicity in the crystals.

Solvent molecules of difluorobenzene and pentane were located in the refinement. The pentane molecule was modelled and restrained to maintain sensible geometries. The disordered difluorobenzene solvent molecule could not be adequately modelled and so was treated using the SQUEEZE algorithm.[7]

Rotational disorder of several CF_3 groups upon the anion was treated by modelling the fluorine atoms over two sites and restraining their geometry.

H1, H2, H3 and H4 were located upon the Fourier map and allowed to refine freely before ride restraints were applied. H1 and H2 in the proximity of rhodium refined to give small U_{iso} values.

Compound 13

H1A, H1B, H1C, H1D, H2, H2C, H2D and H2E were located upon the fourier map and allowed to refine freely.

Table 1: Crystallographic data

Compound	**14**	**17**	**24**	**13**
CCDC No.	970085	970086	970088	970087
Formula	$C_{91}H_{54}B_3F_{48}P_4Rh$ .2.615($C_6H_4F_2$)	$C_{96}H_{68}B_3F_{48}P_4Rh$	$C_{104}H_{114}B_2F_{24}P_4Rh$	$C_{12}H_{30}B_2P_2$
M	2620.90	2392.74	2068.42	257.92
Crystal System	Triclinic	Monoclinic	Triclinic	Triclinic
Space group	*P*-1	*P* 21/c	*P*-1	*P*-1
T [K]	150(2)	150(2)	150(2)	150(2)
a [Å]	16.4783(2)	23.0154(5)	14.9720(10)	6.5693(13)
b [Å]	18.4893(2)	17.2614(3)	17.8931(10)	11.154(2)
c [Å]	21.2720(3)	28.0372(9)	20.0362(12)	11.224(2)
α [°]	79.5983(5)	90	79.893(5)	86.73(3)
β [°]	74.0583(6)	109.424(3)	89.102(5)	81.82(3)
γ [°]	64.6987(6)	90	74.957(5)	89.08(3)
V [Å^3]	5619.05(13)	10504.6(5)	5100.7(6)	812.7(3)
Z	2	4	2	2
Density [g cm^{-3}]	1.549	1.513	1.347	1.054
μ (mm^{-1})	0.344	3.066	2.716	0.244
θ range [deg]	$5.10 \leq \theta \leq 27.47$	$3.06 \leq \theta \leq 76.69$	$3.458 \leq \theta \leq 76.631$	$5.16 \leq \theta \leq 27.45$
Reflns collected	59262	23606	55163	6562
R_{int}	0.027	0.027	0.094	0.0156
Completeness	96.6 %	98.8 %	97.7 %	99.1%
No. of data/restr/param	24841 / 2492 / 1756	20116 / 1216 / 1504	17589 / 988 / 1324	3691 / 0 / 177
R_1 [$I > 2\sigma(I)$]	0.0629	0.0650	0.0753	0.0355
wR_2 [all data]	0.1857	0.1711	0.1900	0.0923
GoF	0.8277	0.9470	0.9080	1.055
Largest diff. pk and hole [eÅ^{-3}]	1.33, -1.14	1.44, -1.32	1.63,-1.31	0.72, -0.27

References

1. J. Cosier and A. M. Glazer, *J. App. Cryst.*, 1986, **19**, 105-107.
2. Z. Otwinowski and W. Minor, in *Macromolecular Crystallography, Pt A*, 1997, vol. 276, pp. 307-326.
3. L. Palatinus and G. Chapuis, *J. Appl. Crystallogr.*, 2007, **40**, 786-790.
4. P. W. Betteridge, J. R. Carruthers, R. I. Cooper, K. Prout and D. J. Watkin, *J. Appl. Crystallogr.*, 2003, **36**, 1487.
5. *Crysalis Pro.*, (2011) Oxford Diffraction Ltd, Abingdon, England.
6. G. M. Sheldrick, *Acta Cryst.*, 2008, **A64**, 112.
7. A. Spek, *J. Appl. Crystallogr.*, 2003, **36**, 7-13.